

α -Alumina and Spinel React into Single- Phase High-Alumina Spinel in < 3 seconds During Flash Sintering

David Kok[†], Devinder Yadav[‡], Emanuele Sortino[‡], Scott J. McCormack*, Kuo-Pin Tseng*, Waltraud M. Kriven*, Rishi Raj[‡] and Martha L. Mecartney[†]

[†]Department of Chemical Engineering and Material Science, University of California, Irvine, CA

[‡]Department of Mechanical Engineering, University of Colorado at Boulder, CO

*Department of Material Science and Engineering, University of Illinois at Urbana-Champaign, Urbana, IL

Abstract (Limit 200 words)

In-situ X-ray diffraction measurements at the Advanced Photon Source show that α -Al₂O₃ and MgAl₂O₄ react nearly instantaneously, and nearly completely to form single-phase high-alumina during voltage-to-current type of flash sintering experiments. The initial sample was constituted from powders of α -Al₂O₃, MgAl₂O₄ spinel, and cubic 8 mol% Y₂O₃-stabilized ZrO₂ (8YSZ) mixed in equal volume fractions, the spinel to alumina molar ratio being 1:1.5. Specimen temperature was measured by thermal expansion of the platinum standard. These measurements correlated well with the black body radiation model, using appropriate values for the emissivity of the constituents. Temperatures in the 1600-1736°C were reached during the flash, which promoted the formation of alumina-rich spinel. In a second set of experiments the flash was induced in a current rate method where only the current flowing through the specimen is controlled and increased at a constant rate. In these experiments we observed the formation of two different compositions of spinel, MgO•3Al₂O₃ and MgO•1.5Al₂O₃, which evolved into a single composition of MgO•2.5 Al₂O₃ as the current continued to increase. In summary, flash sintering is an expedient way to create single-phase, alumina-rich spinel.

1. Introduction

Flash sintering of diverse types of ceramics have shown that rapid densification can be achieved within seconds with the application of an electric field, at furnace temperatures significantly lower than those required for conventional sintering.¹⁻¹¹ Two- and three-phase ceramics have demonstrated a similar rapid densification behavior.¹²⁻¹⁴ Under special circumstances, flash sintering has been shown to induce phase transformations in both single phase ceramics as well as in ceramic composites.^{8, 15-17}

The mechanism of flash sintering remains controversial, but it is generally agreed that the current flowing through the specimen produces significant Joule heating, raising the specimen to significantly above the furnace temperature.¹⁸⁻²⁰ An equation to estimate the sample temperature during flash sintering, using a black body radiation (BBR) model, is given by:¹⁶

$$\frac{T}{T_o} = [1 + \frac{1000W_V}{e_m\sigma T_o^4} \left(\frac{V}{A}\right)]^{1/4} \quad (1)$$

where T is the specimen temperature, T_o is the furnace temperature, W_V is the power density expended in the specimen in units of mW mm^{-3} , e_m is the emissivity, $\sigma = 5.67 \times 10^{-8} \text{ W m}^{-2} \text{ K}^{-4}$ is the Stefan Boltzmann constant, and V/A is the volume to surface area of the specimen in units of mm . In the present work we pay special attention to the emissivity being material and temperature dependent.

In-situ experiments of X-ray diffraction at synchrotrons have been successfully employed to measure the specimen temperature directly using platinum as the standard by calibrating the shifts in the platinum (111) peak against the handbook value of its thermal expansion¹⁹. These experiments have also been used to characterize the phase transformation during flash. In the

present work such phase transformations are observed in real time, at a time scale of about 3 seconds, in a three-phase composite constituted from equal volume fractions α -Al₂O₃, MgAl₂O₄ spinel and cubic 8 mol% Y₂O₃-stabilized ZrO₂ (8YSZ). It follows earlier work where it was shown that flash sintering promoted the formation of high-Al₂O₃ spinel.¹⁷ Here we show the formation of single-phase high-alumina spinel in two types of flash experiments; one carried out in the usual way by applying an electric field and switching to constant current upon the onset of the flash, and the second, a new method where the entire experiment is carried out under current control, but where the current is increased at a constant rate.

These studies of flash in multiphase ceramics may have applications in functional as well as in engineering ceramics.^{21, 22}

2. Materials and Experimental Procedure

Powder compacts were fabricated with equal volumes of the three phases: cubic 8 mol % yttria stabilized zirconia (8YSZ) (Tosoh TZ-8YS), spinel (Baikowski S30CR) and alumina (Taimei TM-DAR). The spinel and alumina had a molar ratio of approximately 1:1.5, which is equivalent to one-third volume fraction of each of the three powders. Powders were pressed into dog-bone shaped samples for flash sintering experiments in our laboratory.¹⁷ Smaller samples were pressed to be approximately 4 mm x 1.6 mm x 1 mm rectangular bars for the *in-situ* synchrotron XRD flash experiments. The dog-bone specimens were pre-sintered for 1 hour at 600°C for 1 h to a green density of 52%, while the rectangular specimens were pre-sintered for 1 hour at 900°C to a density of 55%.

3. Results

3.1 Laboratory Experiments

Flash sintering experiments that were carried out in our laboratory as in described previously.¹⁷ The electrical field was applied to the sample as a step function and, then, the power supply was switched to current control at the onset of the flash when the current suddenly rises. These are described as an electric field control-to-current experiments, and are referred to as Type L. The purpose of these laboratory experiments was to determine the influence of the current density on the evolution of the spinel phase. The conditions for these experiments are listed in Table I as L1, and L2.

3.2 Advance Photon Source Experiments

In-situ experiments were conducted at beamline 33BMC of the Advance Photon Source (APS) at Argonne National Laboratory (ANL). Platinum wires were wrapped around both ends of the length of the sample, and platinum paste (SPI Supplies, West Chester, PA) was applied to ensure good electrical contact. A thin sliver of platinum paste (1 mm wide) was applied to one side of the samples to measure the sample temperature.

The platinum wires were connected to a power supply (DLM 300-2, Sorenson, San Diego, CA) and a digital multimeter (Model 2000, Keithley, Cleveland, OH). The samples were heated inside a quadrupole lamp furnace (QLF). All experiments were conducted at furnace temperature held constant at 1250°C.²³

The sample was placed on an alumina sample holder for stability and was then positioned in the hot zone of the furnace. The QLF was also configured to allow for the incident x-ray beam to travel through the sample and the diffracted beam to impinge on a Pilatus 100K 2D

image plate detector (DECTRIS Ltd, Villigen, Switzerland). The wavelength of the X-ray beam was set to 0.7749 Å (16 kV) for all the *in-situ* experiments. Due to the physical size of the detector, the angular collection range of the detector was 4°. Data was recorded in total scan mode or local scan mode. In total scan mode, the detector traverses the full range of 2Θ. In local scan mode, the detector remains fixed at a specific 2Θ angle and captures the diffracted peaks with 4°. Local scan mode allows for more rapid scans (one scan per 3 seconds). Due to the fast sintering times of flash sintering, *in-situ* data could be collected only in the local scan mode. PDF files for cubic 8YSZ (# 00-030-1468), spinel (# 00-021-1152) and alumina (# 01-070-7346) were converted to the synchrotron radiation wavelength and used for peak identification and indexing.

The shift in the (111) platinum peak was measured in the total scan mode, and converted into specimen temperature using the standard values for the thermal expansion of platinum.²⁴ This baseline temperature calibration was obtained by heating the sample to different temperatures without applying an electric field. The calibration curve is shown in Fig 1. The sample temperature during flash sintering was determined from this curve. Note that a platinum standard was necessary because of the evolution of different phases, with different lattice parameters^{17, 25}.

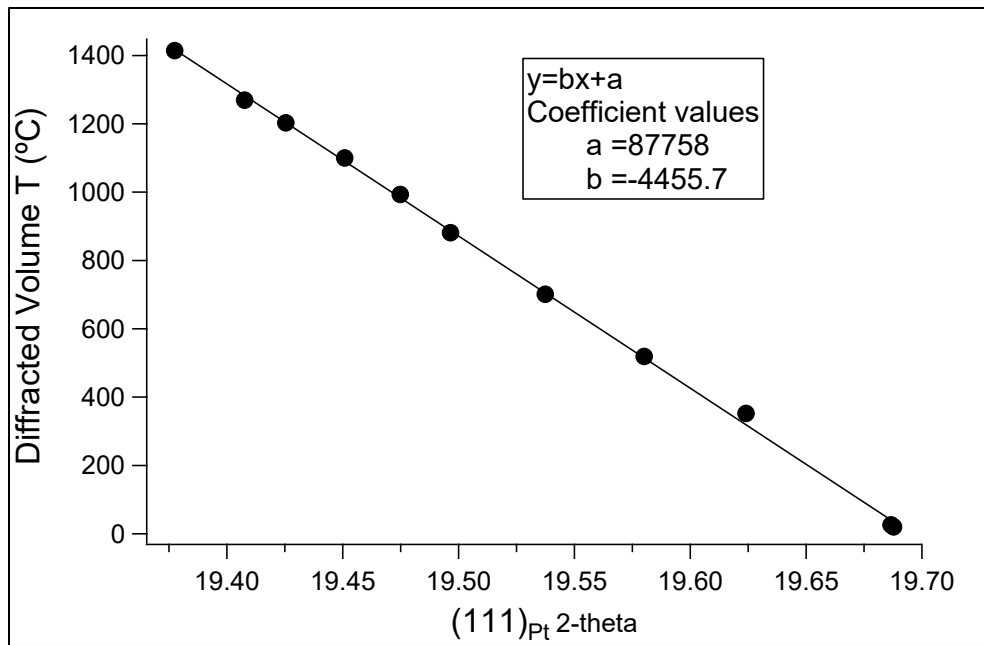


Figure 1. The calibration of the specimen temperature measured by the shift of the (111) peak of platinum.

Flash sintering experiments at APS began by heating the furnace with the sample in position for 5 minutes to allow for equilibration of the sample temperature at 1250°C. Two categories of flash experiment were conducted. The first set of experiments utilized the same flash sintering profile that was done in the laboratory experiments; a voltage control to current limiting profile; these experiments are called Type A. The magnitude of the electrical fields and the current limit for these experiments are given as A1 and A2 in Table I. The diffraction data for A1 was obtained in the total scan mode, with scans being taken before and after the flash. In the case of A2 data were acquired in the local mode at a scan rate of one scan per 3 seconds.

In the second set of experiments only the current flowing through the specimen was controlled (Type B). The current was increased at a constant rate of 25 mA min⁻¹ until it reached the current density of 85 mA mm⁻². Successive local scans were obtained at intervals of 3 seconds. In current-rate experiments the flash sintering process is slower which allows more

detailed analysis of the spinel phase transformation. Table I list the parameters for this experiment under B1.

Table I. List of experiments conducted

Experiment Number	Field (V cm ⁻¹)	Current (mA mm ⁻²)	Flash Type	APS Scan
L1	250	25	A	n/a
L2	250	75	A	n/a
A1	450	75*	A	Total Scan
A2	450	85*	A	Local Scan
B1	n/a	(max current) 85*	B	Local Scan
Type A: Voltage to Current Limit				
Type B: Current Rate of 25 mA min ⁻¹				
*In-situ Experiments at ANL				

4. Results

4.1 Laboratory Experiments (Type L)

For L1 and L2 electric field was held to the same limit of 250 V cm⁻¹, with the current increased from 25mA mm⁻², and to 75 mA mm⁻², respectively. SEM microstructures for shown in Fig. 2. They show that an increase in the current limit resulted in dissolution of the alumina into the spinel phase, as well as in significant grain growth.

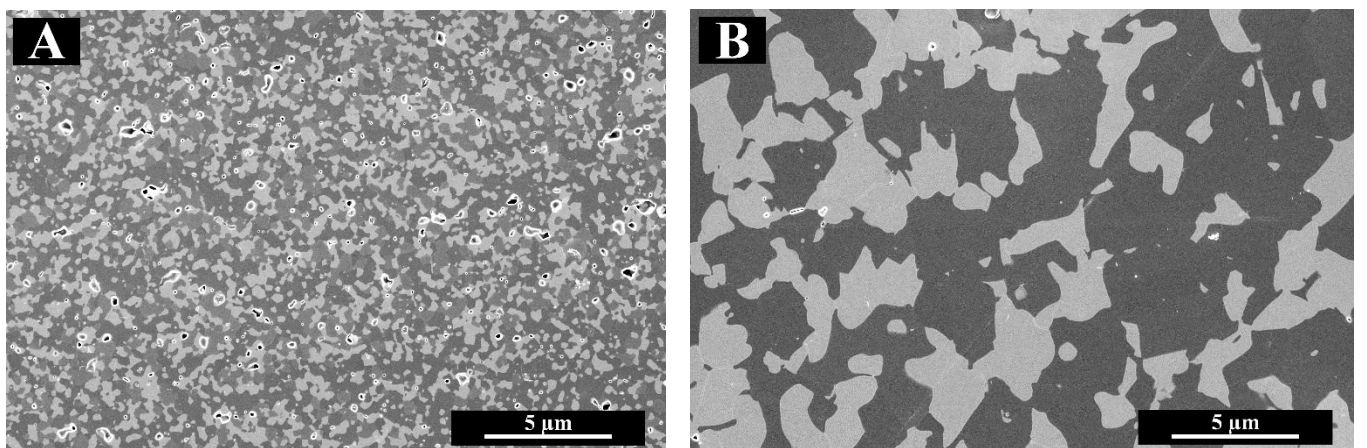


Fig. 2. SEM microstructure of three-phase composites for flash sintered specimens L1 and L2. **(A) L1** - 250V cm^{-1} ; 25mA mm^{-2} . Here the medium dark phase is alumina, the dark phase is spinel, and the light phase is 8YSZ. **(B) L2** - 250V/cm ; 75mA mm^{-2} . The dark phase is high alumina spinel, and the light phase is 8YSZ. Note that the alumina is absent, having dissolved into the spinel phase.

4.2 Advance Photon Source Experiments (Type A)

The total-scan diffraction patterns for experiment A1, taken before and after flash sintering are shown in Fig. 3. The scan before flash sintering shows the three starting phases. However, the alumina peaks are absent in the scan taken after flash sintering; at the same time the spinel peaks are more intense and shifted to the right suggesting a decrease in the lattice parameter. A shift in the zirconia peaks is also seen, and thought to be due to the effect of the dopants.²⁵ The XRD data in Fig. 3 matches previous observations, where high alumina spinel was formed during flash sintering.¹⁷

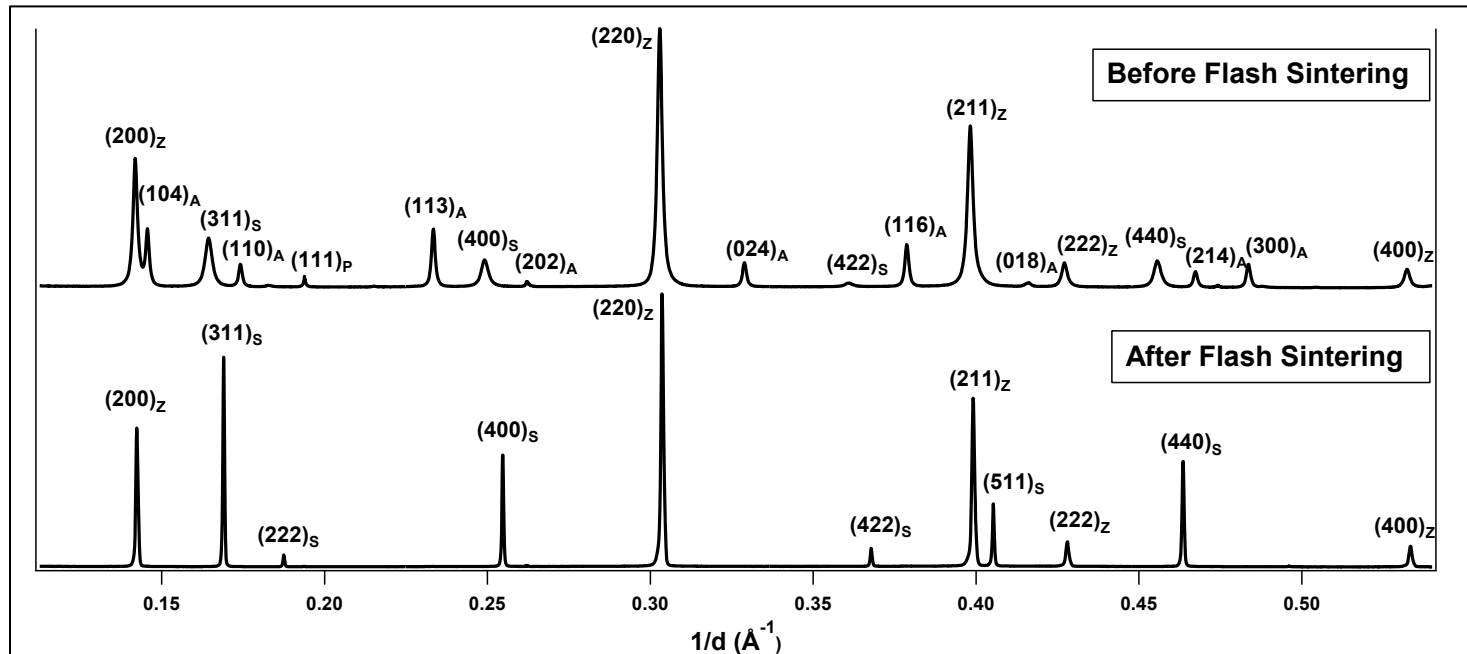


Fig. 3. Synchrotron XRD pattern from before and after flash sintering at 450 V cm^{-1} ; 75mA mm^{-2} . Peaks refer to zirconia (Z), alumina (A), and spinel (S).

The in-situ data for the experiment A2 are shown in Fig. 4. The 2Θ range for the local scan was chosen so that peaks from all three phases, as well as the platinum (111) peak could be included. Note that the dissolution of alumina and formation of high-alumina spinel occurred within one scan, that is within 3 seconds, between the second and the third scan. The formation of high-alumina spinel also corresponds to a large jump in temperature measured with the platinum standard, 1405°C to 1736°C . In A2 residual amounts of alumina can still be seen in Fig. 4, but the bulk of the alumina was consumed in forming the high-alumina spinel.

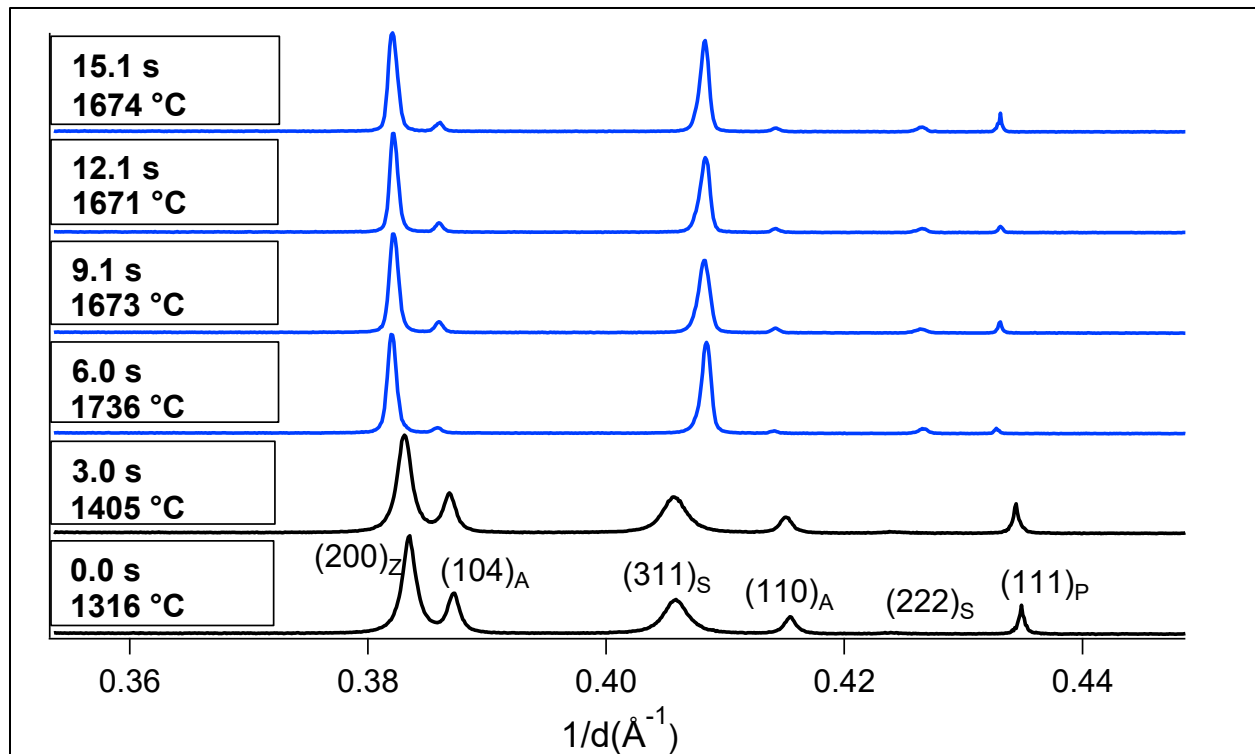


Fig. 4. In-situ synchrotron XRD pattern obtained at 450 V cm^{-1} ; 85 mA mm^{-2} (A2). Peaks have been indexed for zirconia (Z), alumina (A), spinel (S) and platinum (P). Note the dissolution of alumina into spinel between the second and the third scan together with a shift in the (311) peak for spinel to the right.

4.3 Advance Photon Source Experiments (Type B)

In contrast to the Type A experiments where the sintering occurs quickly at the onset of the flash, the process occurs more slowly in Type B experiments where the current is injected and increased at a constant rate. Fig. 5 shows the power density curves for the live experiments; they illustrate the difference between the flash sintering profiles for Type A and B. In voltage-to-current (Type A) experiment the powder density rises quickly at the onset of the flash and reaches a plateau as the power supply is switched to current control. In Type B experiments the power dissipation spikes at the onset of the flash and then continues to rise as the current is increased.

The current-rate experiment slows down the spinel phase transformation, as shown by the data in Fig. 6. Video of the full in-situ XRD scans for this experiment can be found in Supplementary Information. The onset the flash is indicated again by a large increased in temperature of 1384°C to 1526°C (the measurement of the temperatures is described in more detail in the following section), between the scans at 45.5 seconds and 48.6 seconds. As the current increases, the (311) spinel peak splits into two distinct peaks. The intensity of the right peak begins to decrease with time and increasing current density, with the left peak shifting to the right. The double peak evolves into a single (311) spinel peak of the high-alumina spinel phase. Again, a small amount of residual alumina remains. The temperature profiles obtained from the platinum standard are discussed in the following section.

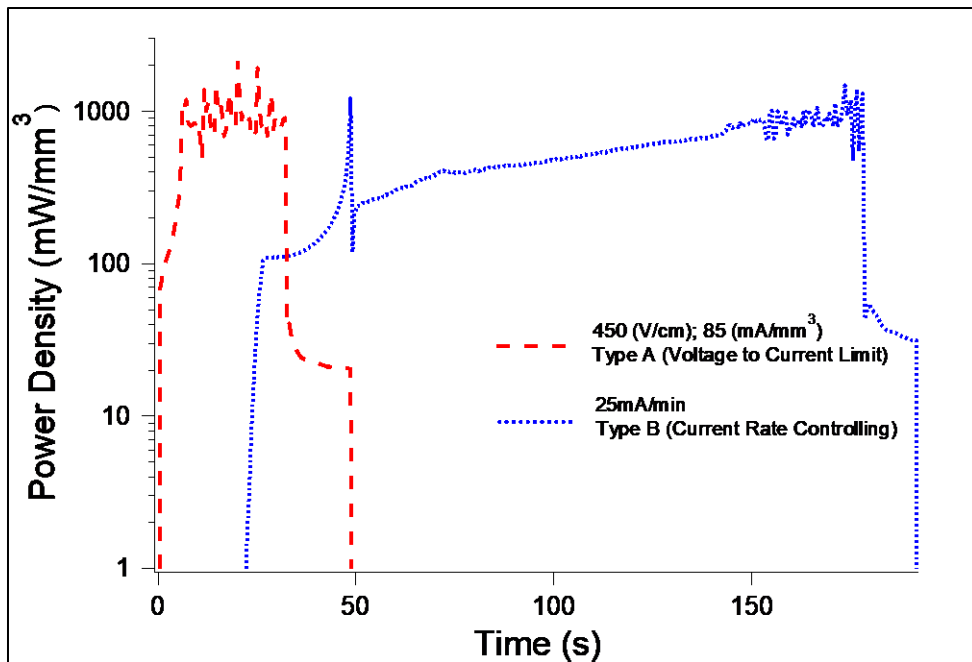


Fig. 5. Power density curve of Type A and Type B flash sintering profiles.

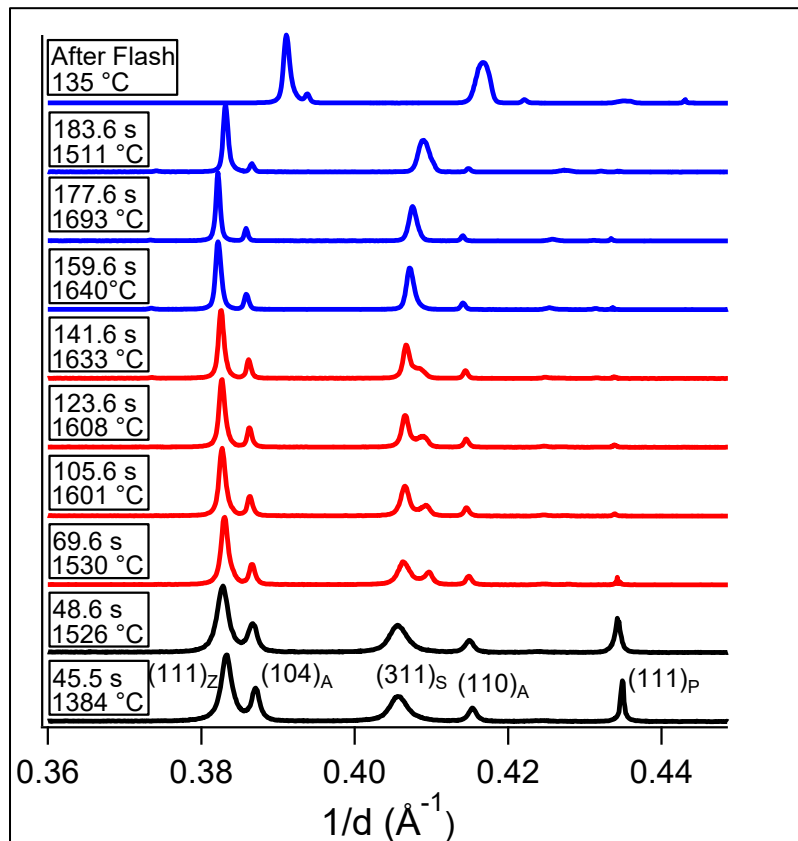


Fig. 6 Selected in-situ synchrotron XRD patterns obtained under Type B current rate controlling flash conditions. Peaks for zirconia (Z), alumina (A), spinel (S) and platinum (P) are shown.

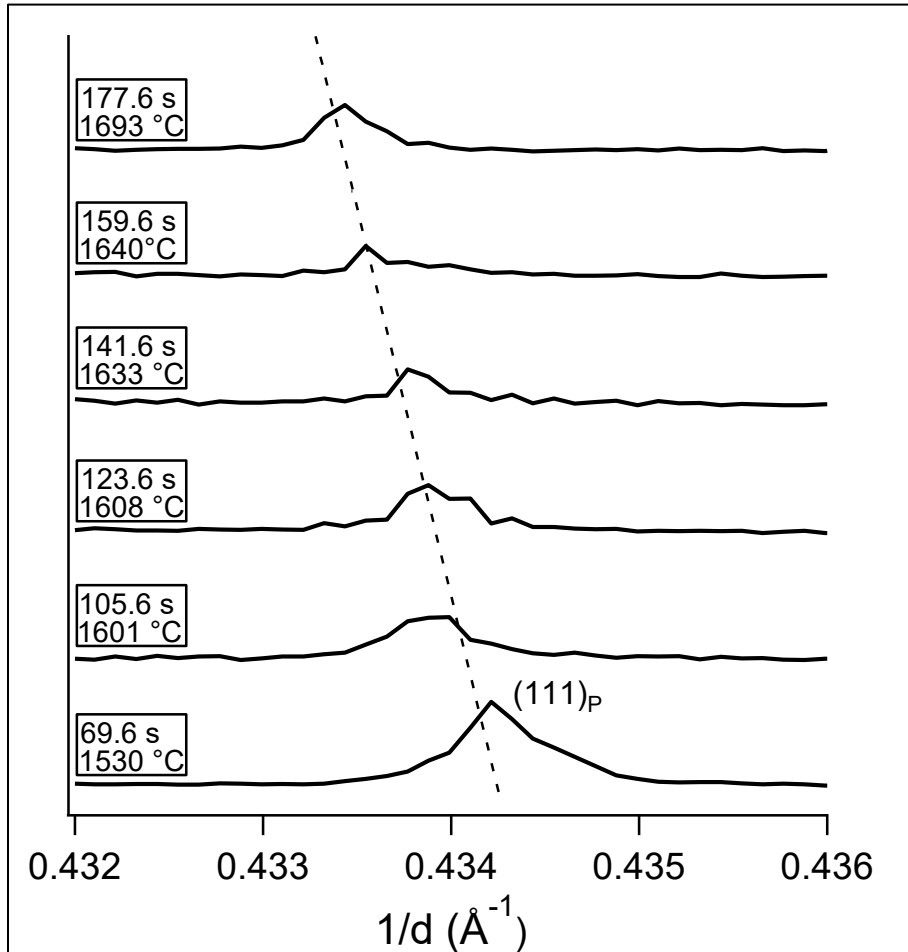


Fig. 7. (111) Platinum peak shift and calculated temperatures during Type B current rate controlling flash conditions.

5. Discussion

5.1 Measurements (Pt standard) and Black Body Radiation Estimate (Eq. 1) of Temperature

In this section we report the best possible estimate of the specimen temperature by two methods, the black body radiation (BBR) model of Eq. (1) and measurements of thermal expansion of the platinum standard.

Both methods have constraints. The BBR model applies only when the specimen is in the steady state, as is the case for Type A experiments where the power density remains at a

plateau. In the current-rate experiments where the power density is constantly increasing the steady state BBR model is not applicable since the electrical energy partitions in to specific heat and into radiation loss. Thus we apply the BBR model only to the experiment A1.

The platinum standard method also has constraints since as shown in Fig. 1 the calibration extends only up to about 1400°C since beyond that platinum paste begins to volatilize and the (111) peak becomes faint, as can be seen in Fig. 6. High magnification of the peak at higher temperatures is shown in Fig. 7. The dashed line shows the extrapolation of the calibration curve from Fig. 1. The extrapolation extends to 1736°C, which is just below the melting point of Pt, 1768°C. These peaks are difficult to resolve, so the results presented for the temperatures estimated from them is subject to a degree of uncertainty. Nevertheless, we present these results for the sake of being as complete as we can.

The application of the BBR model requires knowledge of the emissivity, which is both material and temperature dependent. For YSZ an emissivity value of 0.9 seems appropriate.¹⁹ Literature values for the emissivity values^{26,27} for Al₂O₃ and MgAl₂O₄ were extrapolated to 1600°C; they were 0.47 for Al₂O₃ and 0.19 for MgAl₂O₄. Due to the large differences in the values for the three phases, the rule of mixtures and the inverse rule of mixtures was used to estimate the upper bound and lower bound for the emissivity of the composite; they were 0.52 and 0.35. A lower emissivity value predicts higher specimen temperature since it reduces the energy lost to black body radiation.

In the case of experiment A2 the BBR model is acceptable since the power density reaches a plateau indicating a steady state in the specimen temperatures. The estimated BBR temperature, using the emissivity values given just above, as well as the temperature estimated from the platinum standard are shown in Fig. 8. The Pt-standard method predicts the sample

temperature during the steady state of flash to lie between 1670-1736°C. This range falls within the upper and lower bounds calculated by the black body radiation using the higher and lower values of the emissivity. For comparison the prediction using emissivity of 0.9, the accepted value for zirconia, is also shown; it predicts lower specimen temperature. It is to be noted that the data for emissivity of various materials are not readily available and carry a significant degree of uncertainty.

The current-rate, Type B experiments have the advantage that the sample temperature rises more gradually, being controlled by the rate at which the current is increased. However, being a non-steady state process only the Pt-standard method is applicable. In Fig. 7 the (111) Pt peak is seen to shift as the power density expended in the sample increases. The Pt peaks grow faint above $\sim 1400^{\circ}\text{C}$, and the exploded view of the peaks, shown in Fig. 8, which carries a degree of uncertainty, was used to estimate the specimen temperature.

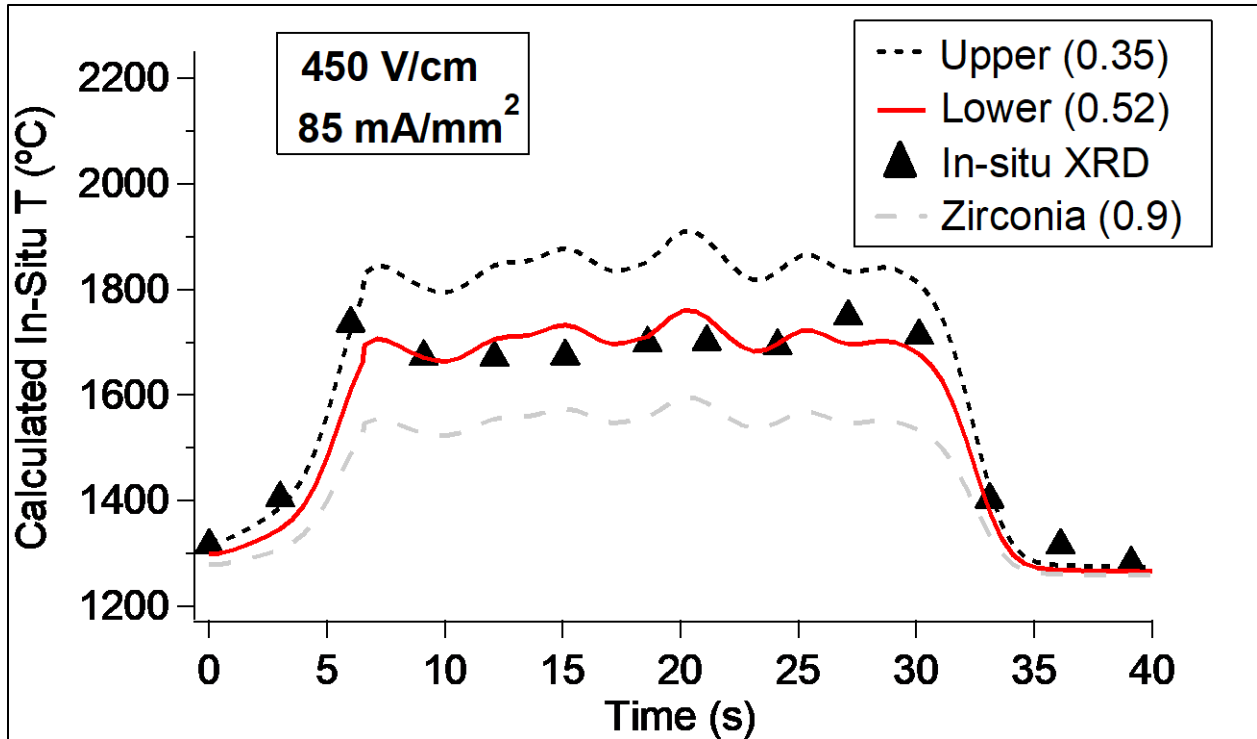


Fig. 8. Calculated black body radiation temperatures for experiment A2 compared with temperatures calculated from in-situ temperatures from the platinum standard. Calculated black body radiation temperatures with zirconia emissivity (0.9) is also shown for reference.

The measurement of the specimen temperature by the Pt-standard method while the power density increases are shown in Fig. 9. The data were obtained from successive local scans. In this plot we see that the specimen temperature rises from about 1485°C to 1525°C at the onset of the flash, and then continues to rise to about 1675°C until the end of the experiment. The dissolution of the α -alumina phase begins at about 1500°C with the development of the second peak for spinel and is completed by about 1640°C. However, measurable amounts of alumina is retained even after the experiment ends and the furnace is cooled down, as shown by the diffraction spectra at the top in Fig. 6.

The comparison between the evolution of the spinel phase is different in Type A and Type B experiments as shown by Figs 4 and 6. In the Type A experiment the transformation is faster and more complete (although some residual alumina still remained) in the Type A

experiment than in the Type B experiment. Furthermore the splitting of the spinel seen in Type B is not seen in the Type A voltage-to-current experiment.

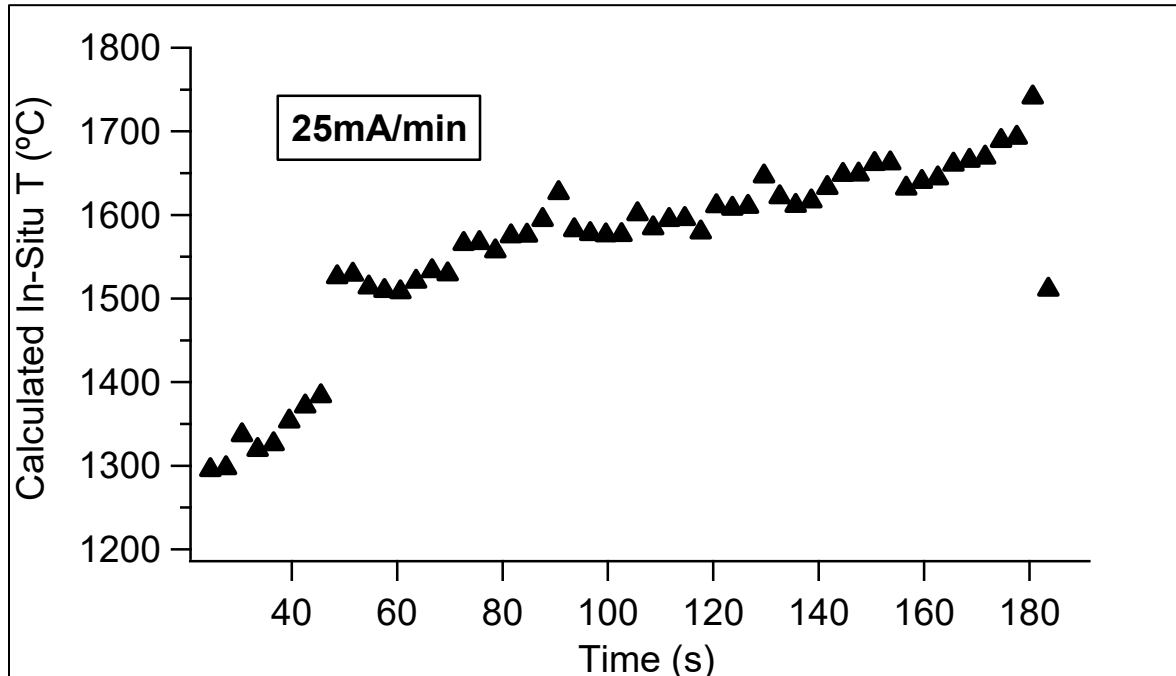


Figure 9. Calculated in-situ temperature from the platinum standard from experiment B1.

5.2 Kinetics of Phase Transformation

The principal result from the present work is the abrupt dissolution of alumina into spinel at the onset of the flash as shown in Fig. 4, in less than 3 seconds. Here we analyze the kinetics of the reaction in terms of a previous study of the reaction between alumina and spinel to form non-stoichiometric spinel.²⁹

Using Fick's second law and the high alumina spinel composition from previous data ($\text{MgO}\bullet 3\text{Al}_2\text{O}_3$), the reaction time could be calculated based on the grain size of spinel.¹⁷ The analysis is based upon Fick's second law,

$$\frac{c_x - c_o}{c_s - c_o} = 1 - \text{erf}\left(\frac{x}{2\sqrt{Dt}}\right) \quad (2)$$

where we insert the following values for the parameters for the present work,

C_x = Conc. At x (0.75 mol% alumina)

C_o = Initial conc. at t = 0 (0.5 mol% alumina)

C_s = Surface con. at x = 0 (1.0 mol% alumina)

x = Distance (surface to middle of spinel grain)

D = Diffusion coefficient (1736°C)

t = Time

The reaction times, calculated from Eq. (2), based on the spinel grain size measured in Fig. 2, are summarized in Table 2. Although the average particle sizes of the three-phase starting material was ~ 250 nm, Fig. 2 shows that the final high alumina spinel grain sizes were much larger, having average grain sizes of $1.5 \mu\text{m}$. The results suggest that the temperature reached during flash sintering in this study may have been sufficient for the formation of high alumina spinel with spinel grain sizes of $2 \mu\text{m}$ and below, with the caveat that the specimen temperature was estimated from faint and rather broad peaks of Pt as shown in Fig. 7.

Table 2. Reaction time to form high alumina spinel based on initial spinel grain size.

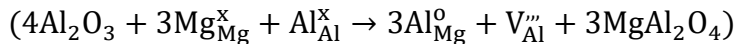
Initial Spinel Grain Size (μm)	Calc. Reaction Time (s)
3.0	5.6
2.0	2.5
1.0	0.6
0.5	0.2

5.3 High-Alumina Spinel Composition

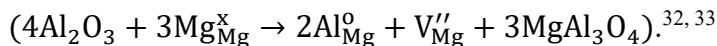
The current rate experiment, B1, was marked by the evolution of two adjacent peaks for (311) spinel. Eventually the two peaks merged into a single peak before the end of the experiment. The lattice parameter of the (311) spinel peaks matched that of a spinel structure having a composition of $\text{MgO}\bullet 3.0\text{Al}_2\text{O}_3$ and $\text{MgO}\bullet 1.5\text{Al}_2\text{O}_3$ at room temperature. This suggested that two separate compositions of non-stoichiometric spinel formed initially. As the

current was increased, the two stoichiometries of the high-alumina spinel converged into $\text{MgO}\bullet 2.5\text{Al}_2\text{O}_3$.

Formation of alumina-rich spinel is due to Al^{3+} occupying Mg^{2+} sites in the spinel structure, but the mechanism by which this defect is charged balanced is under debate.^{30, 31} The defect compensation maybe due to Al^{3+} vacancies:



or by Mg^{2+} vacancies:



Cation incorporation energy calculations have shown that neither mechanism is thermodynamically preferred over another, so that both may occur together.³¹ Flash sintering has been observed to result in the generation of defects in other flash sintered materials.^{3, 34} The formation of non-stoichiometric spinel has also been found to be controlled by the generation of defect clusters.³¹ These defects may explain the formation of alumina-rich spinel when flash sintering the three-phase system of alumina, spinel and 8YSZ.

6. Conclusions

High-alumina spinel can be formed in 3 seconds during flash sintering of composites constituted from equal volume fractions of alumina, spinel and 8YSZ at high current density limits. Under voltage-to-current controlled experiments, with 450 V cm^{-1} and a current limit of 85 mA mm^{-2} , the specimen temperature estimated from the Pt-standard rose up to 1736°C , when the sudden formation of the high-alumina spinel phase was seen. Kinetic analysis shows that it is possible to form high alumina spinel within 3 seconds at such high temperature. However, it

should be noted that the Pt peak position at these very high temperatures has to be estimated from faint and very broad peaks of (111) Pt in the diffraction spectrum.

The black body radiation equation for the estimation of the sample temperature requires the knowledge of reliable values for the emissivity ratio value(s) to achieve accurate results. For example, a change in emissivity from 0.38 to 0.9 can create a spread of approximately 250°C in the uncertainty in the estimate of the specimen temperature.

In the current-rate, Type B experiments the phase transformation occurs more slowly than in the voltage-to-current experiments. Thus, two compositions of alumina rich spinel formed as intermediates ($\text{MgO}\bullet 3\text{Al}_2\text{O}_3$ and $\text{MgO}\bullet 1.5\text{Al}_2\text{O}_3$) during the initial stages of flash, seen in the current-rate (Type B) experiment are not present in the voltage to current (Type A) experiment. However, the two peaks from the dual spinel phase evolved eventually into a homogeneous composition of $\text{MgO}\bullet 2.5\text{Al}_2\text{O}_3$. Further studies are under way to evaluate any residual defect states that may remain in the material as a result of flash sintering.

Acknowledgement

The authors gratefully acknowledge the assistance of Evguenia Karapetrova at Argonne National Lab, Beamline 33BMC where the in-situ synchrotron experiments were performed. This material was based on work supported by the National Science Foundation under Grant No. CMMI MEP 1662791 and U.S. Department of Energy (DOE); Argonne National Laboratory, Grant/Award Number: DE-AC02-06CH11357. DK acknowledges support from the Department of Defense (DoD) through the National Defense Science & Engineering Graduate Fellowship (NDSEG) Program. SEM work was performed at the UC Irvine Materials Research Institute

(IMRI). The University of Colorado Boulder investigators gratefully acknowledge support from the Army Research Office, Grant/Award Number: W911NF-16-1-0200

References

- ¹ M. Cologna, B. Rashkova, and R. Raj, “Flash Sintering of Nanograin Zirconia in <5 s at 850°C,” *J. Am. Ceram. Soc.*, **93** [11] 3556–3559 (2010).
- ² M. Cologna, A.L.G. Prette, and R. Raj, “Flash-Sintering of Cubic Yttria-Stabilized Zirconia at 750°C for Possible Use in SOFC Manufacturing,” *J. Am. Ceram. Soc.*, **94** [2] 316–319 (2011).
- ³ A. Karakuscu, M. Cologna, D. Yarotski, J. Won, J.S.C. Francis, R. Raj, and B.P. Uberuaga, “Defect Structure of Flash-Sintered Strontium Titanate,” *J. Am. Ceram. Soc.*, **95** [8] 2531–2536 (2012).
- ⁴ E. Zapata-Solvas, S. Bonilla, P.R. Wilshaw, and R.I. Todd, “Preliminary investigation of flash sintering of SiC,” *J. Eur. Ceram. Soc.*, **33** [13–14] 2811–2816 (2013).
- ⁵ R. Muccillo and E.N.S. Muccillo, “Electric field-assisted flash sintering of tin dioxide,” *J. Eur. Ceram. Soc.*, **34** [4] 915–923 (2014).
- ⁶ S.K. Jha and R. Raj, “The Effect of Electric Field on Sintering and Electrical Conductivity of Titania,” *J. Am. Ceram. Soc.*, **97** [2] 527–534 (2014).
- ⁷ C. Schmerbauch, J. Gonzalez-Julian, R. Röder, C. Ronning, and O. Guillou, “Flash Sintering of Nanocrystalline Zinc Oxide and its Influence on Microstructure and Defect Formation,” *J. Am. Ceram. Soc.*, **97** [6] 1728–1735 (2014).
- ⁸ A. Gaur and V.M. Sglavo, “Flash-sintering of MnCo₂O₄ and its relation to phase stability,” *J. Eur. Ceram. Soc.*, **34** [10] 2391–2400 (2014).

⁹ Y. Zhang, J.-I. Jung, and J. Luo, “Thermal runaway, flash sintering and asymmetrical microstructural development of ZnO and ZnO–Bi₂O₃ under direct currents,” *Acta Mater.*, **94** 87–100 (2015).

¹⁰ N. Shomrat, S. Baltianski, C.A. Randall, and Y. Tsur, “Flash sintering of potassium-niobate,” *J. Eur. Ceram. Soc.*, **35** [7] 2209–2213 (2015).

¹¹ H. Yoshida, P. Biswas, R. Johnson, and M.K. Mohan, “Flash-sintering of magnesium aluminate spinel (MgAl₂O₄) ceramics,” *J. Am. Ceram. Soc.*, **100** [2] 554–562 (2017).

¹² E. Bichaud, J.M. Chaix, C. Carry, M. Kleitz, and M.C. Steil, “Flash sintering incubation in Al₂O₃/TZP composites,” *J. Eur. Ceram. Soc.*, **35** [9] 2587–2592 (2015).

¹³ A. Gaur and V.M. Sglavo, “Flash Sintering of (La, Sr)(Co, Fe)O₃–Gd-Doped CeO₂ Composite,” *J. Am. Ceram. Soc.*, **98** [6] 1747–1752 (2015).

¹⁴ K.S. Naik, V.M. Sglavo, and R. Raj, “Field assisted sintering of ceramic constituted by alumina and yttria stabilized zirconia,” *J. Eur. Ceram. Soc.*, **34** [10] 2435–2442 (2014).

¹⁵ J.-M. Lebrun, T.G. Morrissey, J.S.C. Francis, K.C. Seymour, W.M. Kriven, and R. Raj, “Emergence and Extinction of a New Phase During On–Off Experiments Related to Flash Sintering of 3YSZ,” *J. Am. Ceram. Soc.*, **98** [5] 1493–1497 (2015).

¹⁶ S.K. Jha, J.M. Lebrun, and R. Raj, “Phase transformation in the alumina–titania system during flash sintering experiments,” *J. Eur. Ceram. Soc.*, **36** [3] 733–739 (2016).

¹⁷ D. Kok, S.K. Jha, R. Raj, and M.L. Mecartney, “Flash sintering of a three-phase alumina, spinel, and yttria-stabilized zirconia composite,” *J. Am. Ceram. Soc.*, n/a-n/a (n.d.).

¹⁸ R. Raj, “Joule heating during flash-sintering,” *J. Eur. Ceram. Soc.*, **32** [10] 2293–2301 (2012).

¹⁹ K. Terauds, J.-M. Lebrun, H.-H. Lee, T.-Y. Jeon, S.-H. Lee, J.H. Je, and R. Raj, “Electroluminescence and the measurement of temperature during Stage III of flash sintering experiments,” *J. Eur. Ceram. Soc.*, **35** [11] 3195–3199 (2015).

²⁰ C.E.J. Dancer, “Flash sintering of ceramic materials,” *Mater. Res. Express*, **3** [10] 102001 (2016).

²¹ H. Sarpoolaky, S. Zhang, and W.E. Lee, “Corrosion of high alumina and near stoichiometric spinels in iron-containing silicate slags,” *J. Eur. Ceram. Soc.*, **23** [2] 293–300 (2003).

²² H. Tang, J. Xu, H. Li, Y. Dong, F. Wu, and M. Chen, “Structure, thermal expansion and optical property of alumina-rich spinel substrate,” *J. Alloys Compd.*, **479** [1–2] L26–L29 (2009).

²³ P. Sarin, W. Yoon, K. Jurkschat, P. Zschack, and W.M. Kriven, “Quadrupole lamp furnace for high temperature (up to 2050K) synchrotron powder x-ray diffraction studies in air in reflection geometry,” *Rev. Sci. Instrum.*, **77** [9] 093906 (2006).

²⁴ R.K. Kirby, “Platinum—A thermal expansion reference material,” *Int. J. Thermophys.*, **12** [4] 679–685 (1991).

²⁵ R.H.J. Hannink, P.M. Kelly, and B.C. Muddle, “Transformation Toughening in Zirconia-Containing Ceramics,” *J. Am. Ceram. Soc.*, **83** [3] 461–487 (2000).

²⁶ G.R. Blair, “Determination of Spectral Emissivity of Ceramic Bodies at Elevated Temperatures,” *J. Am. Ceram. Soc.*, **43** [4] 197–203 (1960).

²⁷ E.D. Palik, *Handbook of Optical Constants of Solids*. Academic Press, 2012.

²⁸ S. Alaruri, L. Bianchini, and A. Brewington, “Effective spectral emissivity measurements of superalloys and YSZ thermal barrier coating at high temperatures using a 1.6 μ m single wavelength pyrometer,” *Opt. Lasers Eng.*, **30** [1] 77–91 (1998).

²⁹ E. Yalamac, C. Carry, and S. Akkurt, “Microstructural development of interface layers between co-sintered alumina and spinel compacts,” *J. Eur. Ceram. Soc.*, **31** [9] 1649–1659 (2011).

³⁰ K.E. Sickafus, J.M. Wills, and N.W. Grimes, “Structure of Spinel,” *J. Am. Ceram. Soc.*, **82** [12] 3279–3292 (1999).

³¹ S.T. Murphy, C.A. Gilbert, R. Smith, T.E. Mitchell, and R.W. Grimes, “Non-stoichiometry in MgAl₂O₄ spinel,” *Philos. Mag.*, **90** [10] 1297–1305 (2010).

³² H. JAGODZINSKI and H. SAALFELD, “Kationenverteilung und Strukturbeziehungen in Mg-Al-Spinellen,” *Z. Für Krist. - Cryst. Mater.*, **110** [1–6] 197–218 (1958).

³³ Y. Okuyama, N. Kurita, and N. Fukatsu, “Defect structure of alumina-rich nonstoichiometric magnesium aluminate spinel,” *Solid State Ion.*, **177** [1–2] 59–64 (2006).

³⁴ J.-M. Lebrun, C.S. Hellberg, S.K. Jha, W.M. Kriven, A. Steveson, K.C. Seymour, N. Bernstein, S.C. Erwin, *et al.*, “In-situ measurements of lattice expansion related to defect generation during flash sintering,” *J. Am. Ceram. Soc.*, n/a-n/a (n.d.).